Journal of Nuclear Materials 390–391 (2009) 869–875

Contents lists available at ScienceDirect

Journal of Nuclear Materials

journal homepage: www.elsevier.com/locate/jnucmat

Particle control study towards burning plasma control in JT-60U

H. Takenaga, The JT-60 Team

Japan Atomic Energy Agency, 801-1 Mukouyama, Naka, Ibaraki 311-0193, Japan

ARTICLE INFO

PACS:
52.25.Fi
52.25.Vy
52.40.Hf
52.55.Fa

ABSTRACT

Study of particle control, such as control of fuel and impurity densities and plasma responses to fuelling and pumping, has been conducted in JT-60U to expand understanding of burning plasma controllability. Peakedness of density profiles increased with decreasing collisionality, which is consistent with ITG/TEM turbulence transport theory. Other control parameters, such as toroidal rotation, existed, i.e. density peaking with counter rotation. Metal impurity accumulation was observed with peaked density profiles, while light impurity accumulation was not observed. Confinement degraded with supersonic molecular beam injections (SMBI), while it was unchanged with high-field-side shallow pellet injection, indicating flexible control using combined fuelling. 2-D divertor simulations suggested that dynamic plasma-wall interaction slows plasma response to divertor pumping. By using the burning plasma simulation scheme, responses of burning plasmas to fuelling were investigated. It was demonstrated to reduce the simulated fusion gain with SMBI due to confinement degradation and flattening of pressure profile.

1. Introduction

Particle control, such as fuel density control, impurity control and recycling control, is one of the critical issues towards burning plasma experiments in ITER. In burning plasmas, the pressure profile modifies the heating profile through α-particle heating, and the heating profile affects the pressure profile through heat transport. Therefore, the degree of 'self-regulation' increases in burning plasmas compared with that in present non-burning plasmas. Fuel density is one of a few controllable parameters in this strong 'self-regulating' system. The 1.5 dimension transport code TOPICS indicates that fusion gain (Q_{DT}) is proportional to square of fuel density ($\sim n^2$) in the range of central ion temperature of $T_i(0)$ = 10–25 keV, when n is changed with constant $T_i(0)$ [1]. The density dependence of Q_{DT} becomes weak, however, when n is changed with constant $HH_{98(y,2)}$. Here, $HH_{98(y,2)}$ is the confinement improvement factor over the IPB98(y,2) ELMy H-mode scaling. The calculation also indicates that Q_{DT} strongly depends on $HH_{98(y,2)}$ and the pressure profile in this $T_i(0)$ range. Taking account of this dependence of Q_{DT}, effective particle control has to be established for flexibility in Q_{DT} towards the first burning plasma experiments in ITER.

This paper highlights recent results of particle control studies in JT-60U towards burning plasma control. In order to establish an effective particle control scenario towards burning plasma control, controllability of density profiles and effects of density profile on impurity transport (Section 2), controllability confinement and pedestal using edge fuelling (Section 3), and controllability of plasma density using divertor pumping (Section 4) were investigated. Furthermore, responses of burning plasma to fuelling were investigated (Section 5) using the burning plasma simulation scheme, where the α-particle heating and the external heating were simulated by two groups of neutral beam injection (NBI). A summary is given in Section 6.

2. Controllability of density profiles and effects of density profiles on impurity transport

Control of density profiles is important for control of burning plasmas, because Q_{DT} strongly depends on pressure profiles. A peaked density profile can produce higher fusion output even with the lower edge density. Many tokamak experiments have indicated that the Greenwald density limits the edge density, but does not restrict the central density. Thus, peaked density profiles have advantage for attaining higher fusion output. However, peaked density profiles might increase impurity accumulation level, because neoclassical transport theory predicts that impurity is accumulated with large density gradient, especially for heavy impurity. On the other hand, although flat density profiles could be favorable for impurity accumulation, high edge density is required to achieve higher fusion output. It is important for establishment of an effective particle control scenario to understand mechanisms for regulating the density profile and effects of the density profile on impurity transport.

Fig. 1(a) shows electron density profiles in JT-60U ELMy H-mode plasmas with the plasma current (I_p) of 1.0 MA, the toroidal magnetic field (B_T) of 2–2.1 T and neutral beam heating power (P_{NB}) of 8–10 MW. The density profile is more peaked in the low

E-mail address: takenaga.hidenobu@jaea.go.jp

0022-3115/$ - see front matter © 2009 Elsevier B.V. All rights reserved.
doi:10.1016/j.jnucmat.2009.01.227

density case (volume averaged density $\langle n_e \rangle$ of 1.5×10^{19} m^{-3}) than in the high density case ($\langle n_e \rangle = 3.4 \times 10^{19}$ m^{-3}). A peaking factor of the density profile decreases from 1.8 in the low density case to 1.3 in the high density case. Here, the density peaking factor is defined by a ratio of the central electron density at $r/a = 0.2$ to the volume averaged density. The edge pedestal structure formed just inside the separatrix depends on the quality of the H-mode. However, in the simplest case with no particle source and constant particle transport coefficients for both particle diffusivity (D) and convection velocity (v), this peaking factor is not affected by the edge boundary condition, because the normalized density gradient ($\nabla n_e/n_e$) is proportional to a ratio of v/D. Therefore, this peaking factor can be considered as a good measure for understanding dependence of density profiles.

In ASDEX-U and JET plasmas, the density peaking factor was shown to increase with decreasing effective collisionality (ν_{eff}) defined as a ratio of the electron-ion collision frequency to the curvature drift frequency [2–4]. The curvature drift frequency, expressed as $\omega_{De} = 2\, k_\perp \rho_s c_s/R$ where $k_\perp$ is a wave number in the direction perpendicular to the magnetic field line, $\rho_s = c_s/\Omega_{ci}$, $c_s = (T_e/m_i)^{0.5}$ and $\Omega_{ci} = Z_i eB/m_i$, provides an estimate of the growth rate for the most unstable mode of drift wave instabilities. In this section, dependence of the density peaking factor on the effective collisionality was first investigated for understanding effects of anomalous inward pinch on density profiles [5]. Here, $k_\perp \rho_s = \sqrt{0.1}$ was used for the estimation of ν_{eff}, which is the same as that in Ref. [2]. This assumption is not much different from the GS2 code calculation in the JT-60U high density ELMy H-mode plasmas, where $k_\theta \rho_s$ (k_θ is a poloidal wave number) was estimated to be 0.4–0.6 for dominant ITG/TEM mode [6]. Fig. 1(b) shows dependence of density peaking factor as a function of ν_{eff}. The density peaking factor increases with decreasing ν_{eff}, suggesting that the anomalous inward pinch driven by turbulent transport due to ITG and/or TEM affects the density peaking. This tendency is similar as that observed in ASDEX-U and JET [2–4]. This dependence indicates that a density profile in ITER should be peaked and also indicates that an increase in density reduces the density profile peakedness, which could weaken the density dependence of Q_{DT}.

Another parameter affecting density profiles was also found, i.e., momentum input or plasma rotation velocity. The effects of momentum input or plasma rotation were investigated in the large volume configuration with various tangential NBI combinations (co-, balance- and counter-), in order to scan the toroidal rotation velocity. The density profile data analyzed here were taken after the installation of the ferritic steel tiles (FSTs) [7]. Therefore, the toroidal rotation velocity range was expanded towards co-direction [8]. The density profile is clearly peaked in the central region for the counter-injection compared with that for co-injection as shown in Fig. 2(a). The edge toroidal rotation was shifted to counter-direction due to fast ion loss as shown in Fig. 2(b). The central toroidal rotation increased in co- and counter-direction depending on injection direction. The toroidal rotation profiles are quite different for both cases in the whole plasma region, although the density profiles are same for both cases in the region of $r/a \geqslant 0.6$. This result indicates that there are other mechanisms for restricting the density profile in the region of $r/a \geqslant 0.6$ and/or that the momentum input or plasma rotation affects the density profile only in the region of $r/a \leqslant 0.6$. The density peaking factors tend to be higher for the counter-toroidal rotation as shown in Fig. 2(c). Here, the toroidal rotation velocity around $r/a = 0.2$ was taken as the abscissa. The toroidal electric field is larger for the counter-injection than for the co-injection in this dataset. However, Ware pinch velocity ($\sim$0.02 m/s at $r/a = 0.3$) is one order of magnitude lower than particle source induced flux velocity (Γ/n), indicating negligible contribution of Ware pinch in determination of density profiles. In a fusion reactor, it is difficult to control the toroidal rotation widely. However, evidence for existence of other parameter dependence of the density peaking factor suggests possibility of density profile control in a fusion reactor.

Neoclassical transport theory predicts that impurity accumulation is stronger for peaked density profiles. Next, carbon and tungsten accumulation was investigated with peaked density profiles. Fig. 3(a) shows carbon density profiles in the high and low density discharges shown in Fig. 1(a). The carbon density profiles measured using charge exchange recombination spectroscopy were almost flat or even slightly hollow for both cases, although neoclassical transport theory predicts inward convection velocity. The peaking factors of carbon density profiles, defined by a density ratio at $r/a = 0.3$ and 0.8, are plotted in Fig. 3(b) and (c) using the same dataset shown in Figs. 1(b) and 2(c). No clear dependence of carbon density profiles on effective collisionality and toroidal rotation was observed. These results indicate no concern of light impurity accumulation even with peaked density profiles in ELMy H-mode plasmas.

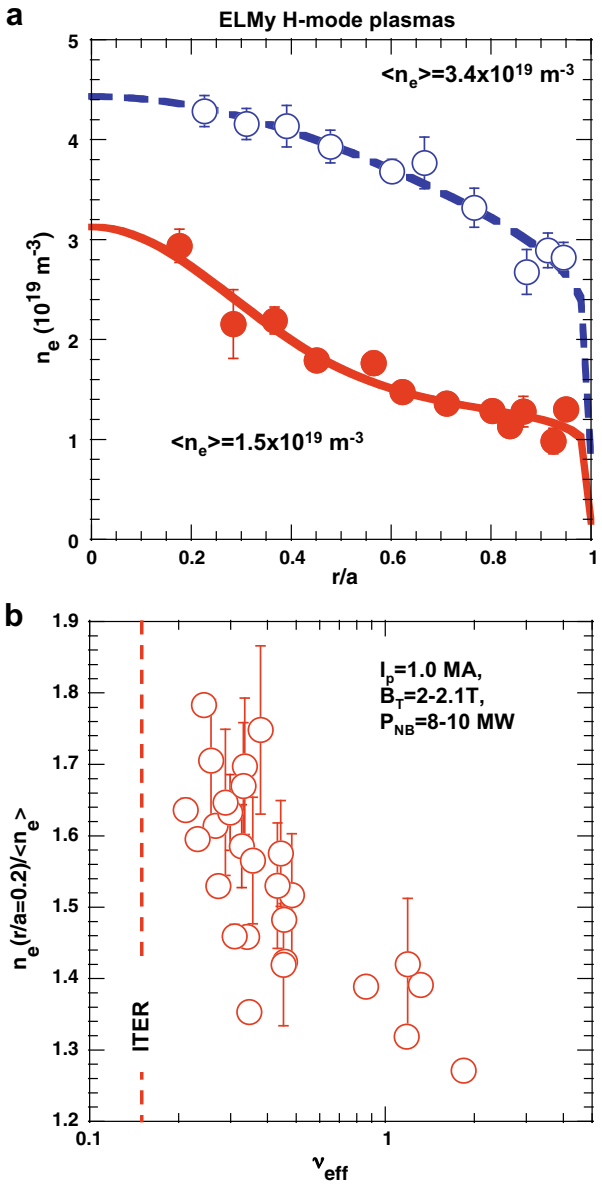

Fig. 1. (a) Typical electron density profiles for low density case (closed symbols and solid line) and high density case (open symbols and dashed line) in ELMy H-mode plasmas. (b) Dependence of the density peaking factor as a function of effective collisionality at $r/a = 0.5$.

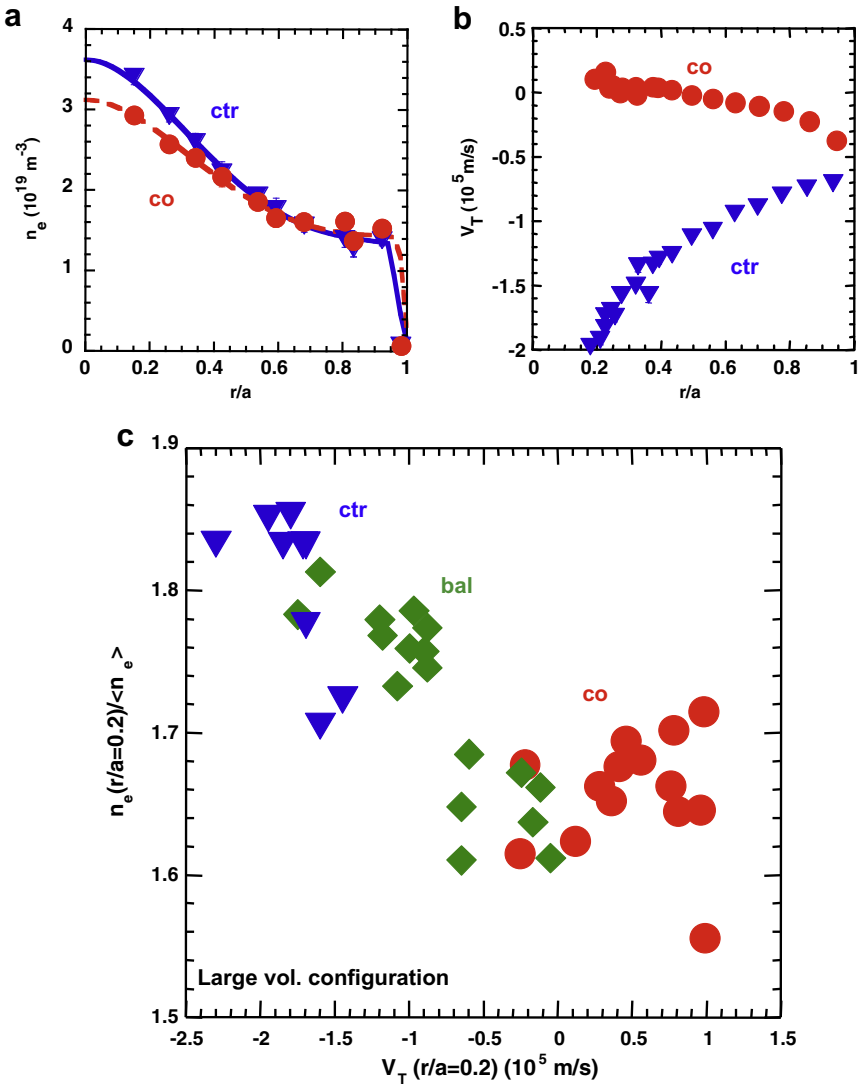

Fig. 2. Profiles of (a) electron density and (b) toroidal rotation for counter-NBI case (reversed triangles and solid line) and co-NBI case (circles and dashed line) in ELMy H-mode plasmas. (c) Dependence of the density peaking factor as a function of toroidal rotation at $r/a = 0.2$. Reversed triangles, diamonds and circles show the data for counter-, balance- and co-NBI cases, respectively.

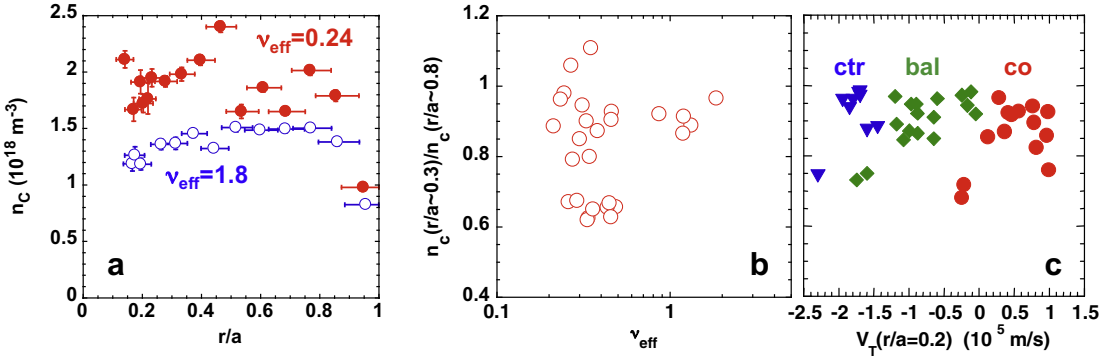

Fig. 3. (a) Typical carbon density profiles for low density case (closed symbols) and high density case (open symbols) in ELMy H-mode plasmas. Dependence of the carbon density peaking factor as a function of (b) effective collisionality at $r/a = 0.5$ and (c) toroidal rotation at $r/a = 0.2$. In (c), reversed triangles, diamonds and circles show the data for counter-, balance- and co-NBI cases, respectively.

The FSTs have ingredient of 8%Cr, 2%W and 0.2%V and cover ~10% of the surface. Therefore, the FST installation allows us to investigate the tungsten accumulation. Note that tungsten is one of the candidates for plasma facing component in a fusion reactor.

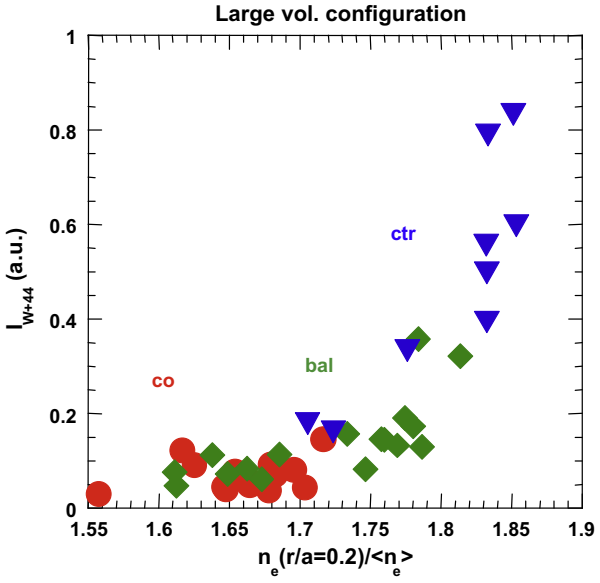

Fig. 4. Dependence of tungsten radiation as a function of toroidal rotation at $r/a = 0.2$. Reversed triangles, diamonds and circles show the data for counter-, balance- and co-NBI cases, respectively.

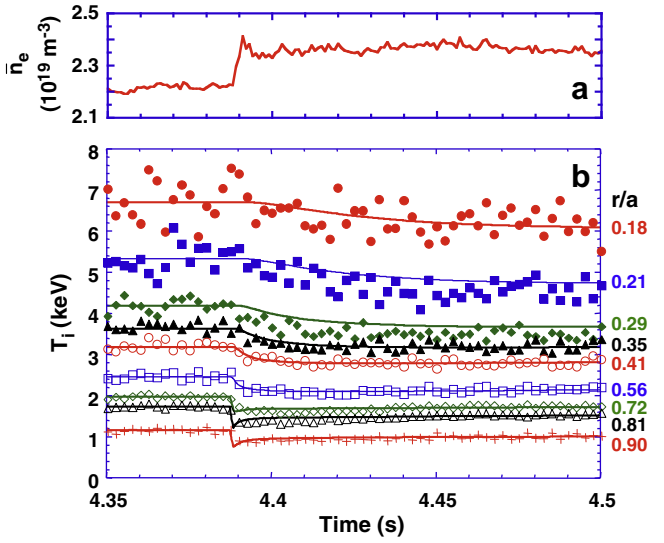

Fig. 5. Time evolution of (a) line averaged electron density and (b) ion temperatures at various radii after SMBI. Solid lines in (b) are calculations using power balance χ_i.

Large tungsten radiation from the core plasma (I_{W+44}) was observed with counter-injection as shown in Fig. 4. The value of I_{W+44} might not be simply proportional to the tungsten density. The time behavior of I_{W+44} shows similar trend to the time behavior of soft X-ray signal. Also, with very high radiation in the central region, the time behavior of I_{W+44} shows similar trend to the time behavior of radiation in the main plasma, while these show different time behavior with relatively small radiation. Therefore, I_{W+44} could be good monitor for the tungsten density in the central region. The tungsten source from the FSTs was not quantitatively estimated, however, it is assumed to be correlated with fast ion loss power to the FSTs. Even at given orbit loss power, I_{W+44} is larger with counter-rotation, suggesting that tungsten accumulation observed here depends on transport or shielding, but not on tungsten source. Heavy impurity accumulation is one of the large concerns with peaked density profiles in ELMy H-mode plasmas. The density profile control should be compatible with a low level of heavy impurity accumulation.

3. Controllability of confinement and pedestal using edge fuelling

In JT-60U, high-field-side (HFS) shallow pellet injections can sustain high confinement at high density, while gas-puffing reduces confinement [9]. By combining these fuelling methods, flexible control of burning plasmas is possible, because Q_{DT} strongly depends on confinement as discussed in introduction. However, plasma response to gas-puffing could be slower and huge amount of gas-puffing is necessary in a fusion reactor. In order to improve controllability, supersonic molecular beam injection (SMBI) has been installed in collaboration with CEA-Cadarache [10]. Injection frequency is less than 10 Hz and duration is ~2 ms/pulse. Gas flow rate was estimated to be ~1.2 Pam^3/pulse at back ground pressure of $P_{BK} = 6$ bar using measurement of increase in gas pressure after SMBI pulses. SMBI speed is expected to be 2.2 km/s at the wall temperature of $T = 150$ °C and $P_{BK} = 5$ bar.

Time behavior of the ion temperature (T_i) was first investigated for understanding SMBI fuelling characteristics. Fig. 5 shows time evolutions of the line averaged density ($\bar{n}_e$), measured with a vertical chord on the magnetic axis, and T_i measured using newly installed fast CXRS system, after SMBI. The value of $\bar{n}_e$ increased by SMBI at $t = 4.39$ s as shown in Fig. 5(a). Number of injected particles was estimated to be about 5×10^{20}/pulse, which is comparable to JT-60U pellet injection. The edge T_i quickly decreased as shown in Fig. 5(b) and cold pulse propagated toward the central region. At $t = 4.4$ s, the T_i decrease has its maximum value at $r/a \sim 0.8$. Therefore, SMBI could directly affect the plasma parameters at $r/a \sim 0.8$, although light from SMBI mainly emitted outside the separatrix. The SMBI speed estimated from the fast TV camera was lower than expected. Ionization front could move slowly towards plasma boundary. The solid lines in Fig. 5(b) shows the time evolution of T_i calculated using ion diffusivity (χ_i) estimated from power balance analysis before SMBI. The time evolution was well reproduced using the power balance χ_i.

Fig. 6(a) shows dependence of the confinement improvement factor over the ITER89P L-mode scaling (H_{89PL}) on the density normalized to the Greenwald density ($\bar{n}_e/n_{GW}$) in high β_p ELMy H-mode plasmas. The accessible density range with $H_{89PL} \sim 2$ was extended to $\bar{n}_e/n_{GW} \sim 0.7$ by maintaining the T_i ITB using the HFS shallow pellet injections. The penetration position of the pellet was estimated to be $r/a = 0.77$–0.84 [9], which is inside the pedestal top. On the other hand, the confinement degraded with gas-puffing due to significant degradation of T_i ITB. Gas-puffed neutral particles almost ionized outside the pedestal top. The confinement also degraded together with the T_i ITB in the case of SMBI, which has intermediate fuelling profiles and directory affects the plasma parameters at $r/a = 0.8$ inside the pedestal top.

The change in confinement is closely related with a strong core-edge linkage [11], that is, improved core confinement (high β_p) enhances the edge pressure and the enhanced edge pressure improves the core confinement. The pedestal pressure was enhanced with the HFS pellet injections, as shown in Fig. 6(b), with keeping high confinement. However, it decreased with gas-puffing to the same level as that in the standard ELMy H-mode plasmas. In the SMBI case, the pedestal pressure is the same level as that in the standard ELMy H-mode plasmas.

In the case of SMBI, the pulse was injected with ~4–10 Hz and transiently decreased central T_i due to SMBI was not recovered. The central T_i decrease was also observed in the pellet injection case, however, it recovered when pellet was not injected in relatively

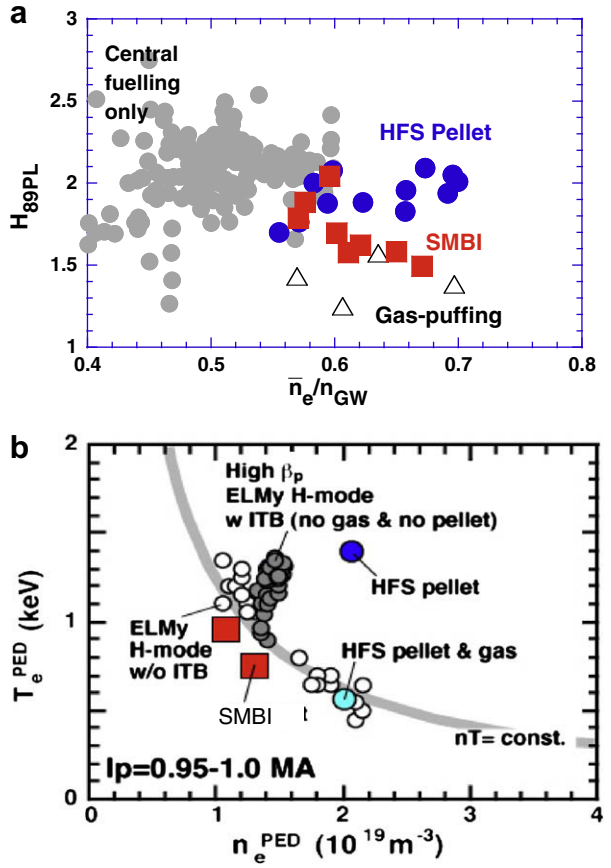

Fig. 6. (a) H_{89PL} as a function of Greenwald fraction. (b) nT-diagram at the pedestal. Closed circles and closed squares show the data for HFS pellet and SMBI, respectively.

long period ($\geqslant$300 ms). By optimizing injection frequency and speed of SMBI, high confinement at high density might be attained with keeping the T_i ITB and enhanced pedestal pressure. If high confinement will be attained with SMBI, SMBI will be powerful tool for burning plasma control. The effects of SMBI on burn control will be discussed later (Section 5) in burning plasma simulation experiments.

4. Controllability of edge density using divertor pumping

Global wall saturation and even outgas from the wall have been observed in the long pulse discharges in JT-60U [12–14]. Behavior of wall pumping can not be understood only using simple static model [15]. Typical example is transient response of wall pumping to divertor pump on [14], where outgas from the wall increased just after divertor pump on as shown in Fig. 7(a). Dynamic plasma-wall interaction could induce increase in degree of 'self-regulating' system and make plasma responses slower to divertor pumping. In order to understand controllability of edge density using divertor pumping, dynamic model is required in addition to static model.

In order to investigate the mechanisms determining the time behavior of the wall pumping, time dependent simulations were performed using the 2-D fluid divertor code UEDGE [16]. Optimized time step width was selected to obtain converged solution at each time step, i.e. long time step width for steady-state phase and short time step width for transient phase. Therefore, longer run time (in real time) was required even for the same time duration (in simulation time) in the case that plasma is largely changed. In the UEDGE calculation, particle and power fluxes at the core boundary (80% of the poloidal magnetic flux) were set to be constant (7.5×10^{20} particles/s and 6.5 MW) as boundary conditions based on the experimental results. Spatially constant anomalous diffusion coefficients were taken for electron and ion thermal diffusivities (χ_e and $\chi_i = 1$ m^2/s) and particle diffusivity ($D = 0.25$ m^2/s). The recycling coefficient at the divertor plates was set to be 0.995 before divertor pump on. The recycling coefficient was changed after the divertor pump on to simulate the divertor pump and dynamic behavior of the wall pumping. The recycling coefficient was divided into three terms, these are static term (R_{st}), dynamic term (R_{dy}) and divertor pump term (R_{pump}). The vale of R_{st} was kept at a constant value (=0.995) even after the divertor pump on. The value of R_{dy} was assumed to increase with increasing heat flux and decreasing particle flux as

$$R_{dy} = C_Q(Q/Q^0 - 1) + C_\Phi(\Phi^0/\Phi - 1).$$

Here, Q and Φ are heat and particle flux to the divertor plates, respectively, and '0' indicates those before divertor pump on. Recycling coefficient is determined by the balance among reflection, trapping (potential and chemical), thermal desorption, and sputtering (physical and chemical). Increase in heat flux could increase sputtering and thermal desorption. Decrease in particle flux could decrease trapping. Dynamic retention was also observed in labora-

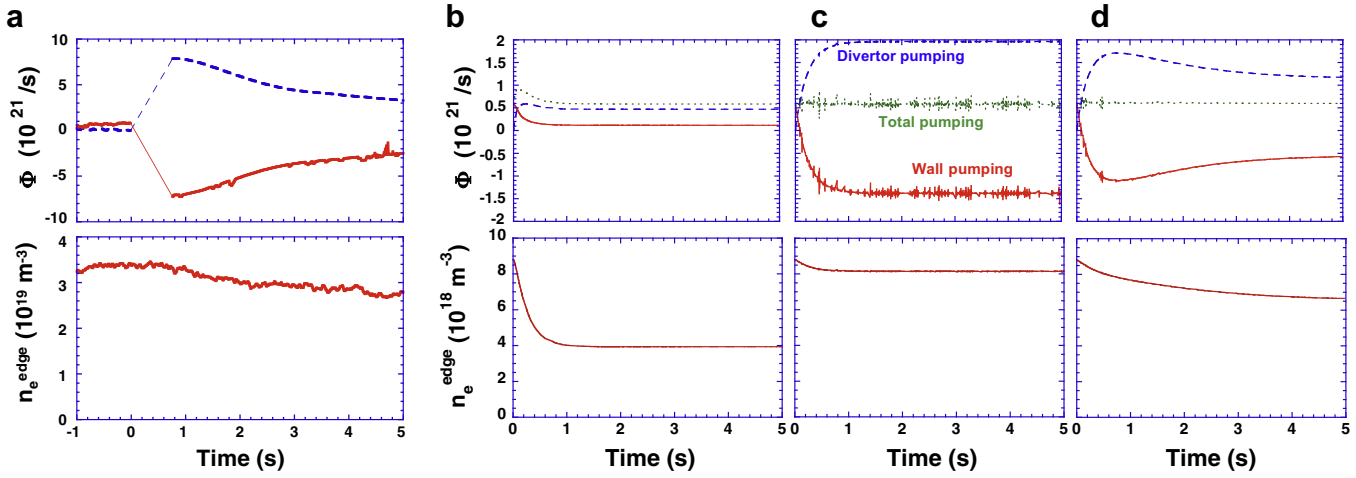

Fig. 7. Upper column: wall pumping (solid line), divertor pumping (dashed line) and total pumping (simulations only) (dotted line), lower column: line averaged electron density (experiment), edge density (simulations). (a) Experiment, (b) $C_Q = C_\Phi = 0$, (c) $C_Q = 0.1$ and $C_\Phi = 0.04$, and (d) $C_Q = 0.08\exp(-t/1.0) + 0.02\exp(-t/100)$ and $C_\Phi = 0.4C_Q$.

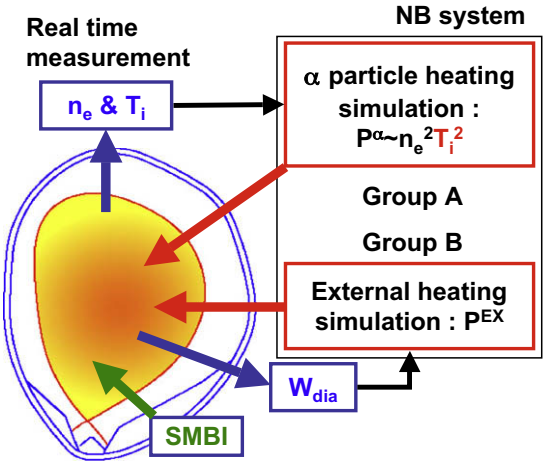

Fig. 8. Schematic drawing of burning plasma simulation scheme.

tory experiments [17]. This recycling model was also used to reproduce the time evolution of the divertor density measured by the mm-wave divertor interferometer during the LH transition [18]. The divertor pump was modelled as $R_{pump} = -0.02(1 - \exp(-t/0.25))$, because divertor shutter is opened for ~1 s. The comparison between the SOL flow measurements and the UEDGE calculation in JT-60U indicated the important role of the drift effects to reproduce the measured particle flow [19]. However, the drift effects were not included in this paper to improve the convergence of the calculation.

We performed the calculation for three cases. In the first case, C_Q and C_Φ were set to be zero, which means no dynamic plasma-wall interaction. In the second case, time constant C_Q and C_Φ were set to be 0.1 and 0.04, respectively. In the last case, time dependent C_Q and C_Φ were set as $C_Q = 0.08\exp(-t/1.0) + 0.02\exp(-t/100)$ and $C_\Phi = 0.4C_Q$. In this case, two time constants of 1.0 s and 100 s were introduced. Fig. 7(b)–(d) shows calculation results for three cases. In the first case (Fig. 7(b)), wall pumping decreased after the divertor pump on, however, it still acts as a pumping. Outgas from the wall was not reproduced. In this case, the edge density decreased by ~50% as the divertor pumping increased. In the second case (Fig. 7(c)), outgas from the wall (negative value) was reproduced and the decrease in density became small compared with that in the first case. In the experiments, outgas from the wall increased once and then decreased as shown in Fig. 7(a), which was not reproduced in the simulation. In the last case (Fig. 7(d)), outgas from the wall increased once and then decreased as well as the experimental results. The results indicated that time dependent C_Q and C_Φ are required for reproducing the experiment, suggesting that wall pumping depends on wall condition, i.e. amount of wall retention. In this case, the density decrease was smaller and slower (as experimentally observed in the line averaged electron density in the main plasma) compared with that in the first results. The dynamic plasma-wall interaction makes the response of edge density to the divertor pumping smaller and slower. In these simulations, changes in the wall pumping and the divertor pumping are smaller than experiments. Quantitative comparison has to be performed in future for the detailed modelling.

5. Burning plasma simulation experiments

In order to extrapolate to burning plasma, a burning plasma simulation scheme has been developed in JT-60U [1,20,21]. Here,

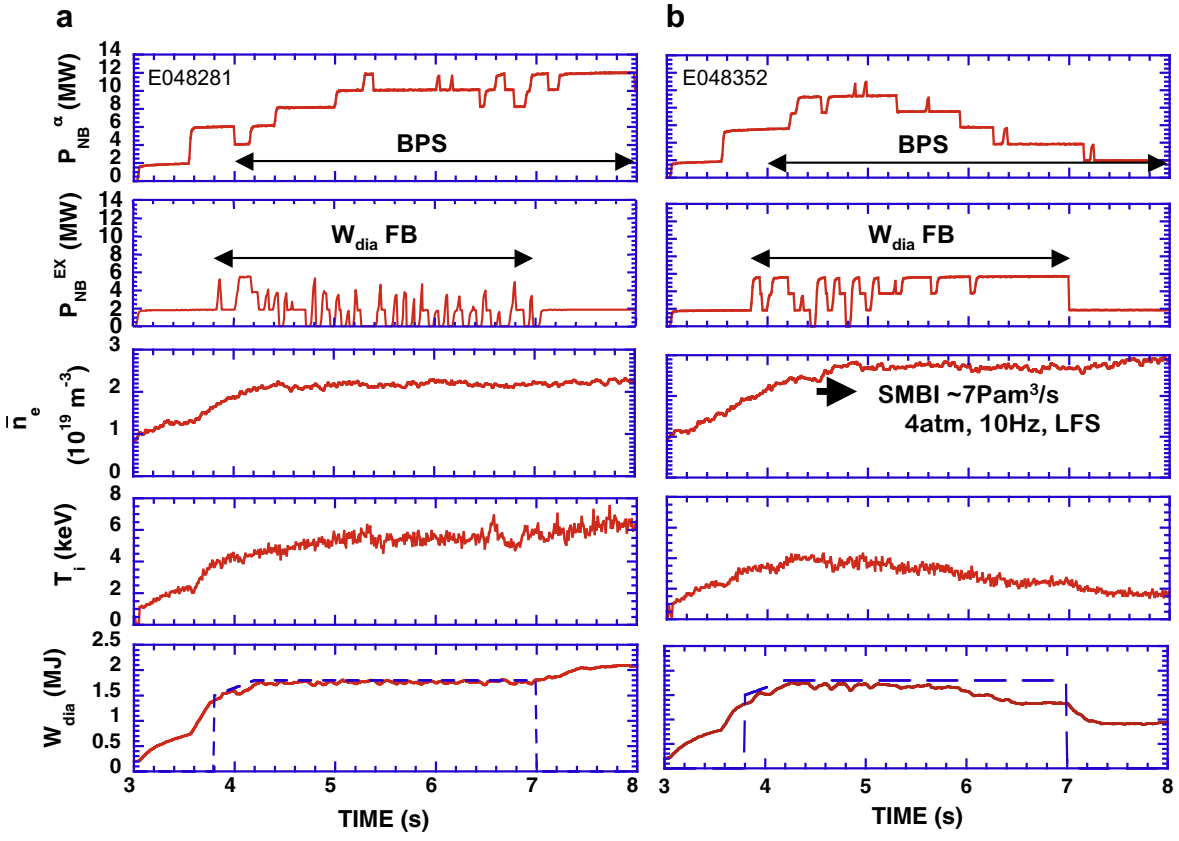

Fig. 9. Waveforms in the burning plasma simulation experiments: (a) without SMBI and (b) with SMBI. First column: the NBI power for α-particle heating simulation, second column: the NBI power for external heating simulation, third column: electron density, fourth column: ion temperature and bottom column: stored energy. The stored energy FB control was applied during t = 3.8–7 s and the burning plasma simulation scheme was applied during t = 4–8 s as shown by arrows. In (b), SMBI was applied from t = 4.5 s.

two groups of NBIs for the simulation of α-particle heating and for the simulation of external heating were used. Although there are limitations for the simulation of the α-particle heating in this scheme, the scheme is still interesting, because linkage between plasma pressure and heating power is simulated. In the scheme used here [1], the heating power for the α-particle heating simulation (P^{α}) was calculated as $P^{\alpha} \sim \bar{n}_e^2 T_i^2$ with consideration of T_i dependence of the DT fusion reaction rate ($\sim T_i^2$) in the range of T_i = 10–25 keV. Due to the limitation of the real-time measurements, the line averaged electron density and the central ion temperature at $r/a \sim 0.3$ were used in this scheme. The schematic drawing of the scheme is shown in Fig. 8. The external heating power (P^{EX}) was determined using feedback (FB) system for the plasma stored energy in this paper for the simulation of burn control using external heating. The fusion gain is defined in this burning plasma simulation scheme as $Q^{sim} = 5P^{\alpha}/P^{EX}$. Here, P^{α} and P^{EX} were taken as a real injected power, because Q^{sim} is introduced for an index of a ratio of α-particle heating power and external heating power.

Fig. 9 shows time evolutions of the discharges in the burning plasma simulation experiments. In Fig. 9(b), SMBI was applied from t = 4.5 s to investigate time behavior of Q^{sim} when the density was increased with confinement degradation. The stored energy FB control by P^{EX} was applied during t = 3.8–7 s for burn control simulation together with the α-particle heating simulation during t = 4–8 s in ELMy H-mode discharges. In the discharge without SMBI (Fig. 9(a)), Q^{sim} increased from 3.7 at t = 4.1 s to 40 at $t \sim 5.8$ s, with the small density change. The value of $HH_{98(y,2)}$ is almost constant (0.87 → 0.83), however, the pressure profile became peaked one ($p(r/a = 0.2)/p(r/a = 0.8) = 8.5 \rightarrow 9.8$) in this period. The stored energy was well controlled at a constant value until t = 7 s by reducing P^{EX} against the increase in P^{α}. After the stored energy FB switched off, the stored energy and α-particle heating increased. In this discharge, although maximum available heating power is limited, increase in α-particle heating could induce thermal runway without burn control. Although the controllability was not lost with $P^{EX} = 0$ in this discharge, the reduction of P^{EX} to zero indicated that the control margin is not so large in high Q region range ($Q \sim 40$).

In order to reduce the fusion gain for keeping the control margin, SMBI was applied to the similar discharge as shown in Fig. 9(b). SMBI decreased Q^{sim} due to confinement degradation from $HH_{98(y,2)} = 0.89$ at t = 4.4 s to 0.72 at t = 6.2 s and flattening of pressure profile from $p(r/a = 0.2)/p(r/a = 0.8) = 9.1$ to 7.9. From t = 6 s, the stored energy can not be kept constant even with maximum available P^{EX}. It is demonstrated to reduce Q^{sim} with SMBI due to confinement degradation and flattening of pressure profile. In future, it is important to demonstrate the flexible simulated burn control by combining pellet injections and SMBI.

6. Summary

Particle control study has been conducted in JT-60U to expand understanding of burning plasma controllability. In order to understand controllability of density profiles, mechanisms for regulating the density profile was investigated. The density peaking factor increased with decreasing the effective collisionality, which is consistent with ITG/TEM turbulence theory. This dependence indicates that a density profile in ITER should be peaked and also indicated that increase in density reduces the density profile peakedness, which could make the density dependence of Q_{DT} weaker. The evidence for existence of dependence of the density peaking factor on other parameter such as toroidal rotation, i.e. density peaking factor increased with counter-rotation, suggests possibility of density profile control in a fusion reactor. Metal impurity accumulation was observed with peaked density profiles, while light impurity accumulation was not observed even with peaked density profiles. Heavy impurity accumulation is one of the large concerns with peaked density profiles. In order to improve the controllability, SMBI was installed, which was expected as a faster response actuator for fuelling compared with gas-puffing. Confinement degraded with SMBI as well as gas-puffing, while it was kept constant with HFS shallow pellets, indicating flexible control using combined fuelling as accelerator and brake. Optimization of SMBI conditions to attain high confinement at high density is future issue for expanding the controllability of SMBI. The dynamic plasma-wall interaction experimentally observed was modelled using the 2-D divertor simulation code UEDGE. The simulations suggested that dynamic plasma-wall interaction makes the plasma responses to divertor pumping smaller and slower. By using the burning plasma simulation scheme, responses of burning plasmas to fuelling were investigated. It was demonstrated to reduce the simulated fusion gain for keeping the control margin with SMBI due to confinement degradation and flattening of pressure profile. In future, it is important to establish an effective particle control scenario using various fuelling methods and divertor pumping for burning plasma control based on the results obtained here.

References

[1] H. Takenaga et al., Nucl. Fus. 48 (2008) 035011.
[2] C. Angioni et al., Phys. Rev. Lett. 90 (2003) 205003.
[3] C. Angioni et al., Phys. Plasmas 10 (2003) 3225.
[4] H. Weisen et al., Plasma Phys. Control. Fus. 48 (2006) A457.
[5] H. Takenaga et al., Nucl. Fus. 48 (2008) 075004.
[6] K.W. Hill et al., in: Proceeding of 19th International Conference, Lyon, IAEA, Vienna, 2002 (CD-ROM file EX/P2-03).
[7] K. Shinohara et al., Nucl. Fus. 47 (2007) 997.
[8] M. Yoshida et al., Plasma Phys. Control. Fus. 48 (2006) 1673.
[9] H. Takenaga, the JT-60 team, Phys. Plasmas 8 (2001) 2217.
[10] H. Takenaga et al., in: Proceedings 33rd EPS Conference Plasma Physics and Controlled Fusion, vol. 30I, European Physical Society, Rome, P-4.112.
[11] Y. Kamada et al., Plasma Phys. Control. Fus. 44 (2002) A279.
[12] H. Takenaga et al., J. Nucl. Mater. 337–339 (2005) 802.
[13] T. Nakano et al., Nucl. Fus. 46 (2006) 626.
[14] H. Kubo et al., in: Proceedings of 21st International Conference Chengdu, IAEA, Vienna, 2006 (CD-ROM file EX/P4-11).
[15] H. Takenaga et al., Nucl. Fus. 46 (2006) S39.
[16] T.D. Rognlien et al., Contribution Plasma Phys. 34 (1994) 362.
[17] K. Matsuhiro et al., in: Proceedings of 18th International Conference Sorrento, IAEA, Vienna, 2000 (CD-ROM file FTP1/22).
[18] H. Takenaga et al., Plasma Fus. Res. 1 (2006) 046.
[19] G.D. Porter et al., J. Nucl. Mater. 313–316 (2003) 1085.
[20] H. Takenaga et al., Fus. Sci. Technol. 50 (2006) 76.
[21] K. Shimomura et al., Fus. Eng. Des. 82 (2007) 953.